Geomechanics for Energy and the Environment 32 (2022) 100368

Contents lists available at ScienceDirect

Geomechanics for Energy and the Environment

journal homepage: www.elsevier.com/locate/gete

A fast approximate method for simulating thermal pile heat exchangers

Fleur Loveridge [a,*], Nicholas Woodman [b], Saqib Javed [c], Johan Claesson [c]

[a] University of Leeds, Leeds, UK
[b] University of Southampton, Southampton, UK
[c] University of Lund, Lund, Sweden

ARTICLE INFO

Article history:
Received 13 December 2021
Received in revised form 30 May 2022
Accepted 1 June 2022
Available online 8 June 2022

Editors-in-Chief:
Professor Lyesse Laloui and Professor Tomasz Hueckel

Keywords:
Ground source energy
Energy piles
Thermal piles
Pile foundations
Heat transfer
Renewable energy

ABSTRACT

Ground source heat pump systems, operating in conjunction with vertical ground heat exchangers, will play a key role in decarbonising heating and cooling of buildings. Design of traditional borehole heat exchangers relies on tools which implement routine analytical relationships between heat transferred and the temperature change in the ground and circulating thermal fluid. However, for novel piled foundations used as ground heat exchangers, there are few such analytical solutions available that are practical for routine implementation. This paper examines the use of a radial approximation to simulate the dynamic thermal behaviour of pile heat-exchangers. Originally developed for small diameter and high aspect ratio borehole heat exchangers, the approach is more challenging for piles since unsteady heat transfer within the pile material is more significant over typical timescales. Nonetheless, we demonstrate that for pile diameters between 300 mm and 1200 mm, generally the error is <1 °C with centrally placed heat transfer pipes or four or more pipes placed near the edge with circumferential spacing less than 550 mm. The radial model is therefore practical for most pile configurations. The strong performance of the model is demonstrated for a year of hypothetical heating and cooling cycles, and also against a field-scale thermal response test.

1. Introduction

The European Green Deal sets out a vision for a carbon neutral EU with net zero emissions by 2050.[1,2] This will facilitate European states to achieve the commitments in the Paris Agreement.[3] In the UK, the Committee on Climate Change has also recommended an emissions target of achieving net-zero greenhouse gases by 2050.[4] This was subsequently passed into law (The Climate Change Act 2008 (2050 Target Amendment) Order, 2019), making it the first country with a legally binding net zero target. Since heating and cooling of buildings accounts for up to 40% of energy use and 20% of emissions,[5] this area must be prioritised for change. Carbon intensity of the UK electricity grid roughly halved since 2014.[6] It is widely anticipated that electrification of heating and cooling using ground source heat pumps (GSHP) will be an important part of the solution (e.g. Refs. 7, 8). However, current barriers to heat pump use include their high capital costs and insufficient capability in the market for drilling the large quantity of ground heat exchangers that will be required to be coupled to the GSHP systems. For new construction, both these challenges can be addressed by achieving dual use of piled foundations as both structural support and ground heat exchangers (GHEs). So called "thermal piles" or "energy piles" have the pipes for the primary thermal fluid circuit for the GSHP system embedded within the pile concrete. This saves on capital costs (e.g. Ref. 9), as well as the energy embodied in construction, and inevitably places the ground-source heat exchanger close to the building where it is needed.

Various arrangements of heat transfer pipes are engineered in practice, typically relating to the underlying construction method of the pile.[10] Where large diameter rotary bored piles are used, the heat transfer pipes are usually located on the pile steel reinforcement cage, which tends to be 50 mm or 75 mm from the edge of the pile. Concrete is then poured into the pile with the cage and pipes in situ. However, where piles are constructed using a Continuous Flight Auger (CFA) method, the fluid pipes tend to be located towards the centre of the pile, arranged around a steel reinforcement bar for stability. This is because the steel cage, which rarely needs to extend the full depth of the pile, is placed after the concrete. Therefore, to obtain full depth pipe installations, it is practical to plunge the pipes into the concrete with an additional full depth steel bar. Both these arrangements are summarised in Fig. 1 (parts a and b). Additional arrangements,

* Corresponding author.
E-mail addresses: f.a.loveridge@leeds.ac.uk (F. Loveridge), N.D.Woodman@soton.ac.uk (N. Woodman).

https://doi.org/10.1016/j.gete.2022.100368

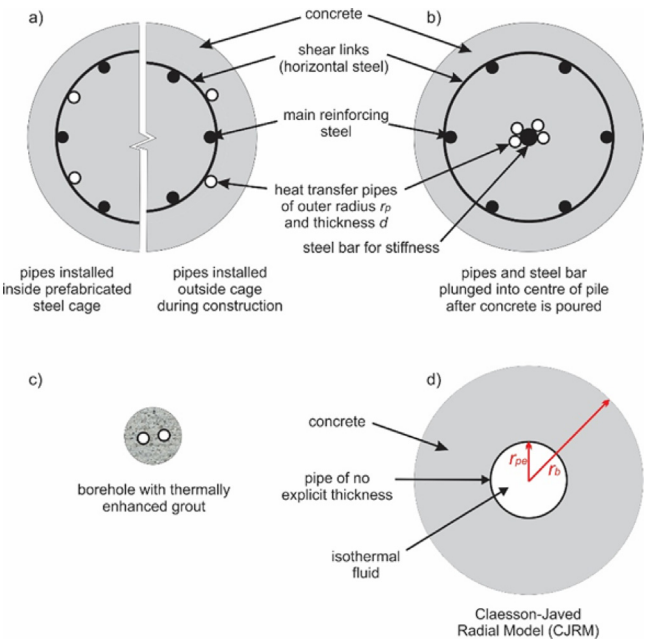

Fig. 1. Typical pile and pipe arrangements for 600 mm diameter (a) rotary bored and (b) CFA type thermal piles, compared with (c) a 150 mm diameter borehole heat exchanger drawn at the same scale, and (d) the Claesson–Javed Radial Model applied for the pile geometries. r_b is the radius of the concrete pile in the ground and r_{pe} is an equivalent radius for the simplified assumption of an equivalent central pipe.
Source: Adapted from Refs. 21, 22

such as the use of the spiral coil heat exchanger are also sometimes used with piles (e.g. Refs. 11, 12). However, in the UK, rotary and CFA types dominate. In all cases, these construction differences give rise to different thermal response characteristics.

Thermal piles potentially offer higher heat transfer rates per drilled metre than conventional borehole heat exchangers[13] due to the ability to include more pipes[14] in the larger cross section of the ground heat exchanger. They have also been shown to offer good system energy efficiencies overall.[15] However, the larger pile cross sectional area also means that the transient heat transport within the pile may cause pile heat exchangers to perform significantly differently to boreholes.[16] Consequently, analytical methods used for the design of boreholes coupled to GSHP systems are rarely applicable when thermal piles are used (e.g. Ref. 17). However, relatively few pile-specific design approaches have been developed. This is in part due to the challenge of dealing with the many potential different pipe and pile geometries that will affect the short term transient thermal behaviour. Prediction methods that include explicitly for the specific geometry of an individual pile tend to be complex in form (e.g. Refs. 11, 18, 19) and hence potentially computationally expensive or hard to access for practitioners. Meanwhile methods which offer simplifications (e.g. Refs. 16, 20) and hence are easier to use, may have lesser accuracy.

As a consequence, there is still a need to develop computationally fast models of thermal piles that remove the need to consider the full pile and pipe geometry explicitly, but yet retain sufficient accuracy over a representative range of timescales. In this paper we make use of an elegant semi-analytical solution for conductive heat flow, which exploits radial symmetry. Here we call this model, the Claesson–Javed Radial model (CJRM). It is detailed in Ref. 23 and in Ref. 22, where the model is tested for typical borehole heat exchanger geometries (e.g. Fig. 1c). In Ref. 24, Woodman et al. first examined the potential of using CJRM for thermal piles. A central thermal store was added to the original radial arrangement, with the intention of accounting for the large mass of concrete that can be present at the centre of a thermal pile. However, the effect of the store was to lower the mid-time temperature, which tended to worsen the match to what occurs with a real geometry.

Therefore, in this paper we examine direct implementation of the original CJRM for piles, focusing on obtaining input parameters that optimise its performance, and quantifying the differences that occur between this approximate approach, numerical simulation of an explicit pile and pipe geometry, and real data. In Section 2 of the paper we detail the CJRM model, and two and three dimensional explicit geometry models. Section 3 presents the results of model comparisons under both constant and varying thermal load conditions, as well as application of CJRM to thermal response test data from a real case study. Finally, we draw conclusions about the cases in which CJRM will be appropriate for application to thermal piles.

2. Method

2.1. Approach

We test the CJRM against a number of conditions of differing complexity, utilising both numerically-generated synthetic datasets for explicit pile and pipe geometries, and also field data.

Firstly, to remove additional complications from axial effects, comparison is made against synthetic data in the 2D plane. This permits examination of model errors arising only from the geometry simplification of the CJRM, without these being masked by any effects that might result from heat flow in the third dimension. At this stage, we examine a thermal step response (often described as a 'G-Function', the relationship between constant applied thermal power and resulting temperature change) for a full range of pile geometries and conductivities.

Secondly, by comparing against synthetic data in 3D we include for axial effects due to the temperature gradient in the heat-exchanger pipes and vertical conduction in the ground and in the GHE. This provides a fuller assessment of the suitability of the model to more realistic conditions, yet still retains assumptions such as homogeneous and isotropic ground conditions. Greater computation expense in three dimensions means only select geometries are considered.

Next, CJRM is compared against time-varying thermal loads applied in three dimensions to investigate the model performance under typical operational conditions. Finally, having built an understanding of both the radial and axial effects under different loading conditions, we apply the model to a field thermal response test (TRT) data set, complete with the variability that comes from fluctuations in power supply and ground heterogeneity than can give spatial variations in thermal properties.

2.2. The Claesson–Javed Radial Model (CJRM)

The two-dimensional CJRM is set out in detail in Ref. 23. A summary is provided in the following paragraphs with implementation equations given in the Appendix. The key assumption made is that the fluid in the multiple heat transfer pipes in the GHE (see Fig. 1a, b, c) are amalgamated to a single fluid-filled pipe. This means that the GHE geometry is simplified to a cylinder, as shown in Fig. 1d, with unchanged external diameter of r_b and an internal diameter of r_{pe}. The fluid sits within the cylinder and is represented by a homogeneous isothermal unit (of radius r_{pe}, refer also to Section 2.6.1) located at the centroid of the ground heat exchanger (Fig. 1d). The fluid is assumed to be uniformly heated by power per unit depth, q_{inj} (W/m). The

pipe that surrounds the fluid is given no explicit thickness in the model, but is still attributed a thermal resistance acting at r_{pe}.

Outside of the pipe there is an annulus of GHE material (i.e. concrete or grout). At the ground heat exchanger wall (at r_b), the thermal medium changes from the GHE material to the surrounding ground.

The temperature above an initially uniform temperature, due to unsteady radial conductive heat flow in the CJRM is described as:

$$\frac{1}{a\,(r)}\frac{\partial T}{\partial t}=\frac{\partial^2 T}{\partial t^2}+\frac{1}{r}\frac{\partial T}{\partial r},\, a(r)=\begin{cases}a_c, & r_{pe}<r<r_b\\ a_g, & r_b<r\end{cases}, \tag{1}$$

where the thermal diffusivity, $a=\lambda/(\rho c)$, in general changes at the ground heat exchanger wall due to differences in both the thermal conductivity (λ) and specific heat capacities (ρc) of the GHE material and the surrounding ground.

The radial heat flux in the ground heat exchanger and ground is given by Fourier's law in radial co-ordinates:

$$q=-2\pi r\lambda\frac{\partial T}{\partial r}, \tag{2}$$

where λ depends on the material i.e. for $r_b<r$, $\lambda=\lambda_g$ and for $r_b>r>r_p$, $\lambda=\lambda_c$ where the subscripts g and c refer to the ground and the GHE filling material respectively.

The heat-flux is continuous over the GHE–soil interface and thus,

$$\lambda_g\frac{\partial T}{\partial r}=\lambda_c\frac{\partial T}{\partial r} \tag{3}$$

The quasi steady-state heat-flow through the pipe is given by:

$$T_f-T\left(r_{po}\right)=R_p q\left(r_{pe}\right), \tag{4}$$

where the thermal resistance of the single equivalent pipe is calculated by:

$$R_p=\frac{1}{2\pi N_p\lambda_p}\ln\left(\frac{r_p}{r_p-d}\right)+\frac{1}{2\pi N_p r_p h_p}, \tag{5}$$

where d is the thickness and N_p is the number of pipes in the real geometry. We elect here to neglect the convective resistance (the second term) for simplicity, and given that it is typically an order of magnitude smaller than the conductive resistance (the first term).

The heat balance for the fluid within the pipe is given by:

$$q_{inj}=C_f\frac{\partial T}{\partial t}+q\left(r_{pe}\right), \tag{6}$$

where C_f (J/mK) is the thermal capacity of the fluid per unit depth. Since it is the temperature gain above a particular constant initial value that is simulated, $T_f=T=0$ throughout the model at t = 0.

The heat transfer equations are solved by means of Laplace Transforms, conveniently organised into a thermal network.[22] The Laplace transform of the response to a step in power input is inverted by integrating along a closed path on the complex plane using Matlab R2017a. The resulting equations used to practically implement the CJRM for that step response are given in the Appendix.

Where required, a time-variable power input is simulated by considering the input power signal to be made-up of a series of piece-wise constant heat injections over time steps of duration Δt. The fluid temperature is the superposition of the step-responses due to the change in power at each step, i.e.

$$T_f=\sum_{i=1}^{N}\left(q_i-q_{i-1}\right)\hat{\mathrm{T}}\left[t-(i-1)\Delta t\right], \tag{7}$$

where $q_0=0$ and $\hat{T}$ is the unit step response

Since the time step used in these variable power calculations is of importance to the resulting temperature change determination,[25] in the analysis presented in Section 3 we utilise a small time step (Δt = 0.01 h). This is to ensure that any differences in model performance determined by the analysis are truly related to the model errors and not to time stepping factors.

2.3. Numerical simulation

2.3.1. 2D numerical explicit models (EGM2D)

A finite element model of the pile with a realistic arrangement of pipes is made in 2D (denoted explicit geometry model, 'EGM2D'). Conduction is simulated in a horizontal plane that passes through the pile. By definition, any effects of the ground surface or pile base are excluded. The fluid within the pipes is assumed to be an isothermal unit with uniformly distributed heating. Unsteady-state heat flow is assumed through the pipes, which are placed within the pile at typical construction locations. The unsteady heat equation is cast in Eulerian co-ordinates, i.e.

$$\frac{1}{a}\frac{\partial T}{\partial t}=\nabla^2 T, \tag{8}$$

where $a=a_b$ in the concrete or grout, $a=a_g$ in the ground and $a=a_p$ in the pipe wall.

The EGM2D model shares some of the major assumptions that are also made for the CJRM: heat flow is by conduction only (groundwater advection is neglected), homogeneity (and stationarity) of thermal properties, isotropy. The steel reinforcement bar is ignored.[26] The external lateral boundaries are constant temperature (equal to the initial temperature, 0 °C) and are located sufficiently far away (the model diameter is 25 m) to not influence the heatflow in the simulations. This approach is consistent with previous validated analyses, e.g. Refs. 16, 21.

This system is solved using COMSOL 5.3a (via Heat Transfer in Solid module). Different pile sizes and pipe arrangements were analysed (see Section 2.4). Mesh sensitivity and time-stepping checks were carried out to confirm the appropriateness of the spatial and temporal discretisation. Time-stepping was carried out using an implicit method (backward differentiation formula), with each step adjusted automatically to ensure numerical stability. The final mesh comprised between 40,000 and 45,000 elements depending on the specific geometry with a minimum element size of 0.5 mm. This is consistent with previously validated 2D pile models.[16,21]

2.3.2. 3D numerical explicit models (EGM3D)

A more realistic explicit geometry model is made in 3D (denoted 'EGM3D'). The ground surface is assumed to be non-conducting (i.e. acting as a perfect insulator). While classic borehole heat exchanger models (*e.g.* Refs. 27, 28) and some pile models (e.g., Refs. 16, 20) use a constant temperature ground surface, this is less appropriate when piles are located beneath a building.[29] In such cases, an insulated boundary is a conservative choice for design compared with the classic approach, since the prediction of the heat exchanger's performance is on the pessimistic side. While there is some field evidence of limited heat transfer from buildings to the underlying ground,[30–32] there is not yet sufficient information to apply more specific criteria. Therefore, an insulated condition is considered a simple and reasonable assumption for the base of a building, and is consistent with recent work (*e.g.* Ref. 19).

The base of the model (at depth, $D_a=40$ m) is also assumed to be insulating. The pile has length $D_b=20$ m, so that the overall model vertical dimension is twice the depth of the pile and the lower boundary does not influence the thermal behaviour. The lateral boundaries are constant temperature (set to T=0, the

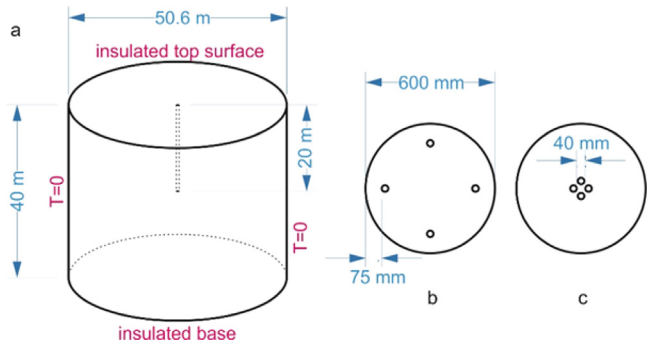

Fig. 2. Geometry and boundary conditions for the EGM3D model: (a) model domain; (b) pile detail for rotary case; (c) pile detail for CFA case.

initial condition) and located 25 m from the pile, again having no influence on the simulation outputs. The geometry and key boundary conditions are summarised in Fig. 2.

In this case only two pile and pipe geometries are considered (see Section 2.4), given the additional computational cost of three dimensions. The pile contains four pipes which are two "u-loops" connected in series. In reality they are connected via header pipes to a heat-pump at the surface. In the simulation this equipment is not included, and the fluid temperature in the pipes is determined according to the heat input q. Frictional heating along the pipe is neglected. Thus, longitudinal heat transfer along the fluid in the pipe is given by the 1D ordinary differential equation:

$$\rho_f A C_f \frac{dT_f}{dt} + \rho_f A C_f v_f \frac{dT_f}{dl} = A\lambda_f \frac{d^2 T_f}{dl^2} + q + q_p, \tag{9}$$

where l is axial distance along the pipe and v_f is the fluid velocity along the pipe. The pipe is a quasi-1D object set into a 3D conducting solid. The source term q is heating (this occurs only along the heat-exchanger at the surface) and the source term q_p is the heat transfer through the pipe wall from the pile (only occurring within the pile). Heat transfer through the pipe wall is quasi steady-state, with the pipe resistance being given by Eq. (5). It should be noted that longitudinal heat transfer within the pipe material is neglected. Again, fluid convection resistance is also neglected, for simplicity, so

$$q_p = \left[T_f - T\left(r_{po}\right)\right]/R_p = \left[T\left(r_{po}\right) - T_f\right] 2\pi\lambda_p / \ln\left(\frac{r_{po}}{r_{pi}}\right). \tag{10}$$

Heat flow in the solid (ground and pile) is as per Eq. (8) for the EGM2D, which has the addition of a q_p sink term which couples the heat transferred between the pipe and the pile. These equations are solved using COMSOL 5.3a (via the 'Heat Transfer' and 'Pipe Flow' modules). Mesh sensitivity and time-stepping checks were carried out to confirm the appropriateness of the spatial and temporal discretisation. Time-stepping was carried out using an implicit method (backward differentiation formula), with each step adjusted automatically to ensure numerical stability. For the CFA and rotary geometries, the selected meshes used approximately 260,000 and 225,000 elements, with minimum element sizes of 0.15 m and 0.2 m respectively. These configurations were chosen to balance model accuracy with computational and memory requirements. Following short term (24 h) testing at 50 kW constant power these models gave average pipe temperatures less than 0.06 °C and 0.21 °C below that calculated using finer meshes. However, at the required longer ($\geq$ 1 year) timescales (see 2.4 below), these finer meshes were too computationally demanding to be manageable, both in terms of run time and memory, even using high performance computing facilities. The consequences of this small temperature underestimation will be discussed in Section 4.

2.4. Specific geometries and material properties

There are three main types of numerically derived synthetic data and one case study of field data that are used here for examining the performance of CJRM. These four analyses are summarised as follows:

(a) **EGM2D vs CJRM** is evaluated by simulated constant thermal load tests using the idealised parameters, given in Table 1, for a range of pile geometries and material properties. Both CFA pipe arrangements and rotary bored pile pipe arrangements were tested. In the former case, either two or four pipes ($N_p = 2, 4$) were assumed to be installed around a 40 mm diameter steel bar. The bar itself was not included in the model, since this would not significantly affect the results.[26] Their arrangement was taken to be symmetrical, although previous work suggests their precise positions will have little bearing on the outcome.[26] For rotary bored piles, up to ten pipes were considered ($N_p = 2, 4, 6, 8, 10$). They were set at different offsets from the pile edge depending on the pile size. For large diameter piles (radius $r_b = 0.3$ m, 0.6 m) then a concrete cover to the pipes and steel of 75 mm was used based on structural recommendations.[33] For smaller diameter piles ($r_b = 0.15$ m), a reduced concrete cover of 50 mm was used as is common in practice to avoid congestion of the steel cage. Additionally, a borehole GHE of $r_b = 0.075$ m was tested for comparison. This is a typical borehole size and therefore the pipes were positioned either in the centre and touching or at the edge (and touching the edge) of the GHE. These correspond to the extreme positions of Ref. 34. Different thermal properties were applied in the concrete and the ground so that their conductivity ratios were either 0.5, 1 or 2. The comparison is run over 10^7 s (115 days) to ensure reaching steady state conditions within the pile.

(b) **EGM3D vs CJRM** is evaluated by comparison with simulated constant thermal load tests using the idealised parameters, given in Table 1 for two 600 mm diameter piles of 20 m depth. One rotary arrangement and one CFA arrangement were used, with four pipes in each case. The concrete to ground thermal conductivity ratio was kept constant at 2. The comparison is run over 10^8 seconds (1157 days).

(c) **EGM3D vs CJRM** is evaluated with a simulated variable thermal load using the idealised parameters, given in Table 1 for two 600 mm diameter piles of 20 m depth (the thermal load is detailed in Section 2.5). One rotary arrangement and one CFA arrangement were used, with four pipes in each case (Fig. 2). The concrete to ground thermal conductivity ratio was kept constant at 2. The comparison is run over 3.15×10^{x7} s (1 year).

(d) **CJRM vs real data** is evaluated for a field thermal response test (TRT) on a 600 mm diameter pile constructed to 31 m depth in London Clay, as reported by Ref. 19. As for the synthetic cases, the pile contained four pipes. The test lasted 1.27×10^{x6} s (353 h, or 14.7 days). Summary details of the test are given in Table 2.

2.5. Thermal loads

For cases (a), (b) and (d) (Section 2.4) constant heating power were applied to the numerical models and to CJRM as indicated in Tables 1 and 2. For the case of varying thermal load application (c), a hypothetical annual heating and cooling cycle is simulated by both an EGM3D and the CJRM. This is composed of daily heating cycles in the winter and daily cooling cycles in

Table 1
Simulation conditions for idealised constant thermal load and cyclic loading conditions. Two generic pile types are simulated: 'CFA' and 'Rotary'. The thermal conductivities of the concrete and ground ($\lambda_c - \lambda_g$) are permuted as (1 - 2); (2 - 1) and (2 - 2).

Item	Geometry	Properties	Comments
Fluid	$r_{pi} = 0.0123$ m.	$\rho_f = 1000$ kg/m^3 $c_f = 4217$ J/kgK $v_f = 0.25$ m/s	Isothermal. Constant total heat injection q_{inj}=50 W/m or varying thermal load as per Fig. 2. Fluid velocity in pipes for EGM3D model
Pipes	$r_{po} = 0.015$ m. $N_p = 2$, 4, 6, 8, 10 uniformly separated. Cover = 50 mm or 75 mm.	$\rho_p = 950$ kg/m^3 $c_p = 1900$ J/kgK $\lambda_p = 0.45$ W/mK	High density polyethylene[35]
Concrete pile/ borehole	Circular cross-section. $r_b = 0.075$, 0.15, 0.3 and 0.6 m Pile depth $D_b = 20$ m (EGM3D)	$\rho_c = 2000$ kg/m^3 $c_c = 800$ J/kgK $\lambda_c = 1$ or 2 W/mK	
Ground	Circular outer model domain ($r_o = 25$ m) Ground domain extends 20 m below base of pile (for EGM3D model)	$\rho_g = 2000$ kg/m^3 $c_g = 800$ J/kgK $\lambda_g = 1$ or 2 W/mK	Initial conditions and outer boundary temperature fixed to $T = 0$ °C to capture changes in temperature.

Table 2
Field Thermal Response Test conditions.[19]

Item	Geometry	Properties	Comments
Fluid	$r_{pi} = 0.0103$ m.	$\rho_f = 1000$ kg/m^3 $c_f = 4217$ J/kgK $v_f = 0.96$ m/s	Circulation fluid is tap-water without additives. Constant heating *Q=1.*69 kW
Pipes	$r_{po} = 0.0125$ m. $N_p = 4$ Shank spacing = 42.5 cm	$\rho_p = 950$ kg/m^3 $c_p = 1900$ J/kgK $\lambda_p = 0.4$ W/mK	Typical values from Ref. 36 and Ref. 19
Concrete pile	$r_b = 0.3$ m Pile depth $D_b = 31$ m	$\rho_c c_c = 2.2$ MK/m^3 $\lambda_c = 0.88$ W/mK	λ_c from back analysis, other parameters assumed[19]
Ground	London Clay which extends beneath base of pile	$\rho_g c_g = 2.4$ MK/m^3 $\lambda_g = 1.48$ W/mK $T_0 = 14.2$ °C	λ_c from back analysis, T_0 from initial TRT circulation, other parameters assumed[19]

the summer. To determine the hour by hour thermal load, an annual sinusoid is multiplied by a daily heating or cooling shape to give an annual pattern (Fig. 3). The heating and cooling shapes simply give the relative amount of heating and cooling in winter and summer respectively, and the total magnitude at any day is determined when they act as multiplier to the sinusoid. As is typical for many commercial buildings the annual heating and cooling energy is balanced. However, the cooling requirement occurs over a shorter time period in each day and at a higher rate. This is reflected in the heating and cooling shapes. The total energy demand applied to the single pile under simulation is therefore 41826 kWh in heating and a further 41826 kWh cooling with peak cooling at 60 W/m and peak heating at 30 W/m (Fig. 3c). These power rates are within typical expected values for energy piles.[13,35,37]

2.6. Equivalence and matching

To apply the CJRM to a particular pile, an equivalent single pipe or radius r_{pe} needs to be derived. This was done via matching the 2D steady state resistance of the concrete pile in the numerical and analytical calculations for the long term using the results of the analysis in (a) and (b) (refer to Section 2.4 above). Additionally, CJRM has been matched to very short time conditions of the numerical model through equivalence of the thermal capacity of the fluid. The results in Section 3 show the magnitude of the deviation of the analytical and numerical models in the critical mid-time period that will be important for energy piles (a few hours to a few days).

2.6.1. Geometry and r_{pe} determination

All aspects of geometry and physics that can be preserved are retained in the CJRM. This includes the GHE material and ground thermal properties and borehole radius (r_b), which are kept the same as for the EGM. The effective radius of the single effective pipe (r_{pe}) is set to provide the identical fluid temperature drop over the concrete pile during quasi steady-state conduction at the end of the constant thermal load simulation (i.e. at t=1 × 10^7 s). This is achieved by computing the averages of T_{po} and T_b around the pile and pipe boundaries and assuming steady-state radial heat-flow at the end of the simulation, i.e.:

$$\overline{T}_{po} - \overline{T}_b = qR_c = \frac{q}{2\pi\lambda_c} \ln\left(\frac{r_b}{r_{pe}}\right). \tag{11}$$

In this study we have determined R_c from the EGM (using the left and side of Eq. (11)). This is to remove R_c estimation from our analysis and focus only on the comparative shape of the resulting step response curves (G-functions). However, in practice, the resistance of the concrete part of the pile, R_c, can be determined by the multipole method.[38,39] A line source approximation to the multipole method is presented in Ref. 40 and has been shown to be sufficiently accurate for many geometry configurations, including piles with $r_b \geq 300$ mm and $r_p \leq 40$ mm, and also smaller energy piles, within certain r_p and N_p ranges. In this case, r_{pe} would need to be determined from Eq. (11) having independently assessed R_c.

2.6.2. Fluid thermal capacity and pipe resistance

The thermal capacity of the fluid, C_f, is made equal to the fluid capacity in the EGM. This is despite the fact that the fluid

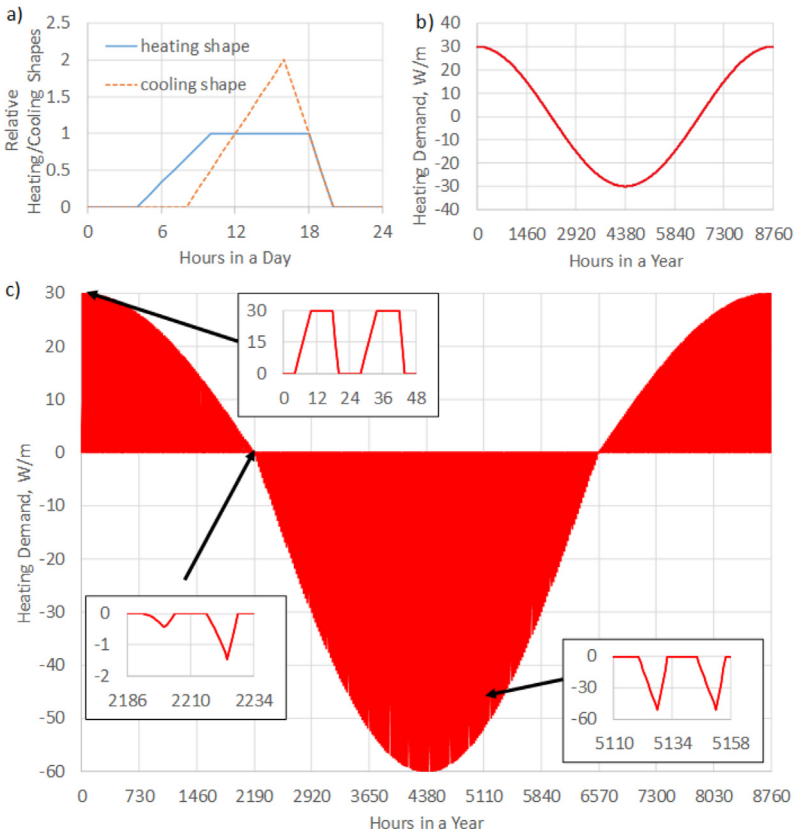

Fig. 3. (a) Daily heating and cooling patterns, expressed in relative unit-less form. Note heating shape used to calculate positive demand, and cooling shape for negative demand. (b) Annual heating demand pattern (cooling is negative). (c) Combined heating demand pattern (cooling is negative).

area changes between the models. Therefore, in effect either the fluid density or specific heat c_f are being changed. The thermal capacity per metre depth is $C_f = N_p \rho_f c_f \pi r_{pi}^2$.

A characteristic time for thermal diffusion within the pipe wall is $\left(r_{po} - r_{pi}\right)^2 / a_p$, which is relatively short (~30 s). Therefore, it is reasonable that the CJRM model assumes steady-state heat transfer in the pipe. Thus, the pipe resistance expected in the EGM is estimated as:

$$R_p = \frac{1}{2\pi\lambda_p} \ln\left(\frac{r_{po}}{r_{pi}}\right) \tag{12}$$

The equivalent pipe resistance for the CJRM is a fraction of that for the EGM since there is only one pipe in the CJRM transmitting the same total power, i.e. $R_{pe} = R_p / N_p$.

3. Results

3.1. CJRM performance in 2D

Table 3 shows the combination of pile sizes, pipe number and positions. Not all the permutations are evaluated, because there are limits under which it is physically possible to fit pipes around a central fixture, and also to reflect common practice. For example, CFA piles typically contain only one or two U-loops only ($N_p = 2, 4$), while for rotary piles the circumferential spacing (CS) of the pipes is rarely below 200 mm. For each of these combinations, Fig. 4 gives the maximum absolute difference (error) in estimated fluid temperatures between the CJRM and EGM2D for 1×10^7 s of constant heating under conditions given in Table 1. For each combination three ratios of thermal conductivities in the borehole and ground respectively ($\lambda_c - \lambda_g$) are used. These are annotated as (1–2); (2–1); (2–2), giving conductivity ratios (λ_c / λ_g) of 0.5, 2 and 1 respectively.

It can be seen that the errors are consistently larger in the case of pipes in rotary pile arrangements (Fig. 4a) compared with the CFA arrangements (Fig. 4b); up to 4 times larger temperature difference. This is to be expected given the greater similarity of the CFA geometry to the CJRM simplified geometry (Fig. 1b and Fig. 1d). For the rotary case the errors increase with the size of the pile and reduce with the number of pipes installed. This is because larger rotary piles with fewer pipes installed are clearly further from the idealised radial geometry shown in Fig. 1d.

For both types of piles, larger errors are associated with a lower concrete to ground thermal conductivity ratio (0.5), while for the higher ratios (1 and 2) the errors are similar. This suggests that the absolute value of GHE material (concrete) conductivity may be more important. This makes sense since lower conductivities will lead to larger temperature changes and hence higher absolute errors.

The absolute values of temperature difference between the two models shown in Fig. 4 will depend on the value of the applied thermal power. This was set at 50 W/m to be in the centre of the range of recommended values,[13,37] and also higher than many field measurements.[35] For these reasonable conditions, the absolute error remains less than 1 °C for all the CFA pile geometries and many of the rotary pile geometries where the circumferential spacing is within typical ranges.

Figs. 5 and 6 plot the dimensionless temperature response of the different cases calculated using the CJRM and EGM2D models. In this case dimensionless temperature (Φ) is defined as:

$$\Phi = 2\pi\lambda_g \Delta T_f / q, \tag{13}$$

and dimensionless time (Fourier number, Fo) as:

$$Fo = \alpha_g t / r_b^2. \tag{14}$$

Table 3
Matrix of EGM2D vs CJRM comparison conditions.

No. pipes \\Pile size	Ø150 mm [r_b = 75 mm]	Ø300 mm [r_b = 150 mm]	Ø600 mm [r_b = 300 mm]	Ø1200 mm [r_b = 600 mm]
2	Borehole (Pipes at edge; CS=188 mm) Borehole (Pipes touching)	Rotary (CS = 267 mm) CFA	Rotary (CS = 660 mm) CFA	Rotary (CS=1602 mm) CFA
4	*N/A*	Rotary (CS=134mm) CFA	Rotary (CS=330 mm) CFA	Rotary (CS=801 mm) CFA
6	*N/A*	*N/A*	Rotary (CS=220 mm)	Rotary (CS=534 mm)
8	*N/A*	*N/A*	*N/A*	Rotary (CS=401 mm)
10	*N/A*	*N/A*	*N/A*	Rotary (CS=320 mm)

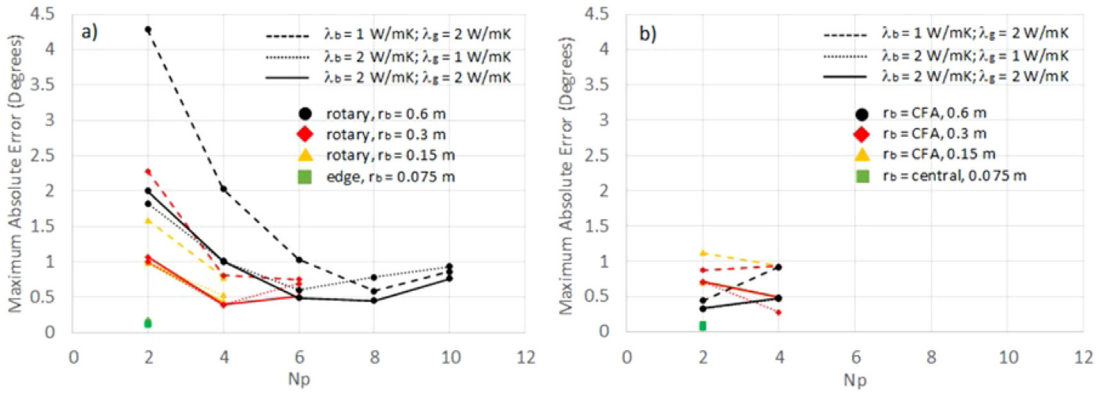

Fig. 4. Maximum differences (absolute error) between the predicted fluid temperatures from the CJRM and EGM2D for the cases set out in Tables 1 and 3 and for three thermal conductivity ratios (λ_c/λ_g = 0.5,1,2). (a) Rotary bored pile configuration. (b) CFA pile configuration.

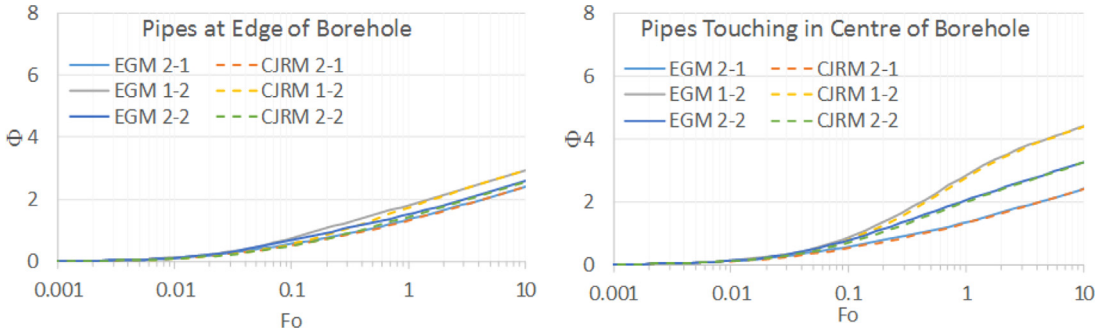

Fig. 5. Dimensionless temperature response (G-function) for typical borehole geometry r_b =75 mm , N_p = 2 calculated using the CJRM and EGM2D models. Refer to Tables 1 and 3 for full parameter and geometry conditions.

3.1.1. Borehole geometries

Fig. 4 showed that the CJRM is comparatively accurate for typical borehole GHE geometries (*i.e.* in the case where the borehole radius is small compared to typical pile cross-sections). In Fig. 5, it can be seen that these maximum differences are relatively small compared to the temperature changes over the period, and they occur in the period between *Fo*=0.01 and 1. This is to be expected given previous results,[22] which showed maximum errors of 0.2 °C when validating the method against a large scale sandbox experiment. In our analysis, the greatest difference in predicted fluid temperatures is 0.18 °C (Φ = 0.023), and occurs where there is a wider pipe spacing and when borehole and ground conductivities of 1 and 2 W/mK are assumed. The CJRM approximation is therefore likely to be of adequate accuracy for many applications with boreholes of these dimensions. In the subsequent sections, we quantify the increasing errors with large diameter piles, and examine the times scales for these errors.

3.1.2. Impact of pile size

Fig. 6 shows how the accuracy of the CJRM changes for simulating increasing radius for piles installed with four pipes. It can been seen that as the pile radius increases, the shapes of the temperature response curves for the two models change. This is the source of the increased errors shown in Fig. 4. In particular, at intermediate timescales (*Fo* = 0.01 to *Fo* = 1), as the diameter of rotary piles increases the deviation of the two models grows. The worst case is for pile and ground conductivities of 1 and 2 W/mK respectively, which for a 1200 mm diameter rotary pile

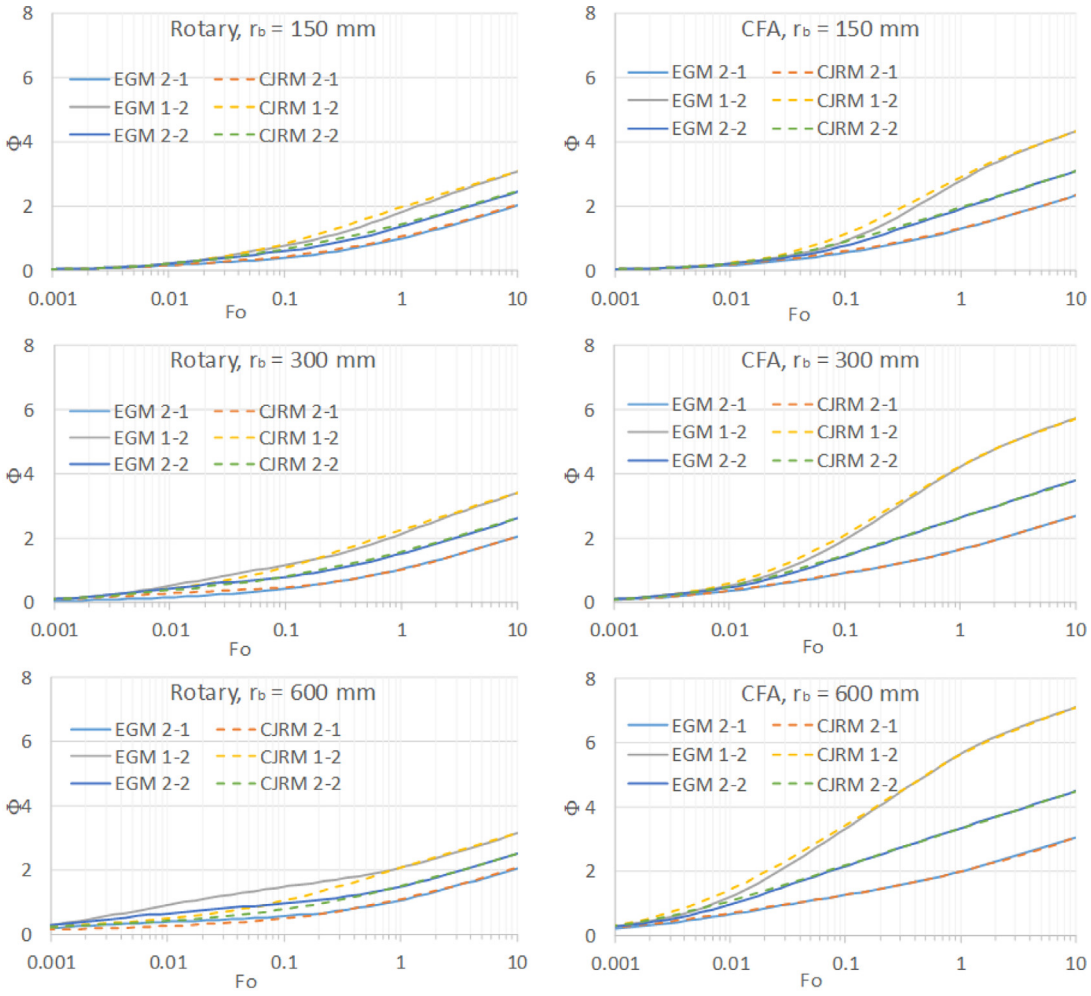

Fig. 6. Dimensionless temperature response (G-function) for typical rotary (left) and CFA (right) pile geometries at (from top to bottom) 150, 300 and 600 mm radius piles and $N_p = 4$, calculated using the CJRM and EGM2D models. Refer to Tables 1 and 3 for full parameter and geometry conditions.

with four pipes results in a maximum error of 2 °C ($\Phi = 0.51$) at a time of just under 3 h ($Fo = 0.035$). This represents an error of 41% compared with the EGM2D temperature at that time. For the rotary cases the CJRM always underestimates the temperature change at the point of maximum error.

For CFA piles, the maximum mid time error occurs for the smaller diameter pile (300 mm), also for pile and ground conductivities of 1 and 2 W/mK. The maximum error is 0.93 °C ($\Phi = 0.23$), occurring at just over 1 h (Fo=0.013). In these cases CJRM tends of overestimate the temperature change compared with the EGM.

At short and long times the temperatures predicted by both models converge. This is because the matching process (Section 2.5) ensures long- and short-time asymptotic convergence of the step responses. The long-term (i.e. for Fourier number, $Fo > 5$) fluid temperature approaches a straight line on a semi-logarithmic temperature–time graph, *i.e.* $T_f \sim \frac{q_{inj}}{4\pi\lambda_g}\left[\ln\left(\frac{4a_g t}{r_b^2}\right) - 0.5772\right] + q_{inj}\left[R_p + R_c\right]$. This is the long term asymptotic behaviour of the classical infinite line source model (*e.g.* Refs. 27, 41). The short-term fluid temperature change is initially also linear, i.e. $T_f \sim qt/C_f$.

3.1.3. Impact of number of pipes installed

For CFA piles the errors between CJRM and EGM are relatively small and not strongly dependent on the number of pipes installed (Fig. 4). This is not the case for rotary piles, where the number of pipes strongly effect the appropriateness of the single pipe approximation in CJRM. Fig. 7 shows the temperature response curves for four cases of 1200 mm diameter rotary piles with differing numbers of pipes from $N_p = 4$ to $N_p = 10$. This illustrates how the mid time deviation reduces as the number of pipes increases, and also occurs at earlier times.

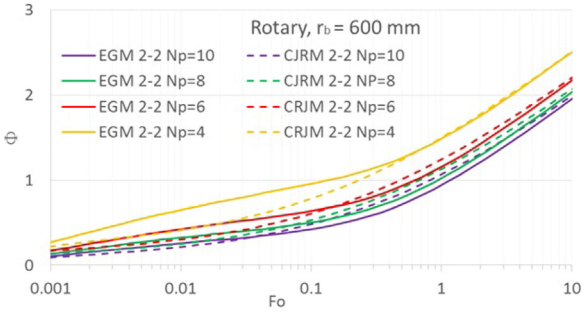

Fig. 7. Dimensionless temperature response (G-function) for a 1200 mm diameter rotary pile with different numbers of pipes, calculated using CJRM and EGM2D. Refer to Tables 1 and 3 for full parameter and geometry conditions.

Generally the maximum error occurs between 1 h and 3 h (Fo = 0.01 to 0.05). It can be up to 2 °C for $N_p = 4$ (pile and ground conductivities of 1 and 2 W/mK respectively), but

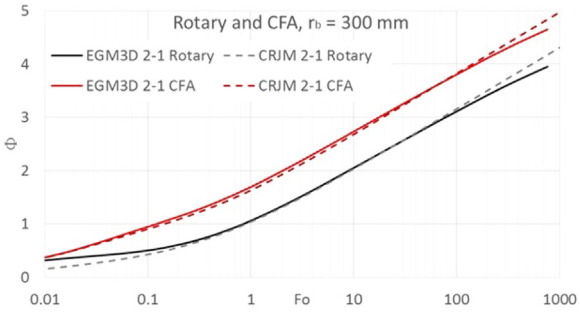

Fig. 8. Non dimensional temperature response (G-function) for 600 mm diameter piles with four pipes under constant thermal load of 50 W/m; $\lambda_c = 2$ W/mK.; $\lambda_g = 1$ W/mK.

reduces to less than 1 °C once more pipes are installed so that the circumferential pipe spacing is less than 550 mm. In terms of Φ, the errors are up to 0.5 for $N_p = 4$ and between 0.1 and 0.25 for other cases.

3.2. CJRM performance in 3D

3.2.1. Constant thermal load

The 2D analysis above neglects axial heat flow. As times approach $\sim D_b^2/4a_g$ axial conduction towards the base of the pile in EGM3D will cause the temperature response curve to deviate from the semi-log asymptotic temperature of CJRM. Furthermore, the temperature gradient in the pipes (which will depend, amongst other controls, upon the fluid velocity in the pipes) will also cause the temperature distribution in the pile to deviate from the 2D idealisation. These effects can be seen in Fig. 8, where substantial deviation between the two models occurs once Fo >100. At $Fo = 10$ the difference is less than 1 %, while at $Fo = 100$, the difference remains less than 2%.

The precise time of divergence between the models will depend on the aspect ratio (ground heat exchanger length to diameter ratio), AR. In this case we present AR=33 (Fig. 8). This is fairly typical for piles, but values can be as low as 15 or greater than 50.[42] As in the two dimensional analysis, the CFA piles show lesser difference between the EGM and the CJRM at smaller times (Fo <0.5). However, in the long term the difference will depend only on the aspect ratio and not on the pile internal geometry. At the end of the analysis (just over 3 years, $Fo = 763$), the difference between the CJRM and EGM3D is $\Phi = 0.2$ in both cases, representing 4 % and 5 % of the EGM3D total for the CFA and rotary cases respectively. Larger differences would be expected for less advantageous conductivity ratios, but at these timescales the differences are still small compared with the mid time deviations (Section 3.1).

Divergence is also expected to increase over longer timescales, with most energy pile design conducted over design lives of several decades. However, this analysis is limited to identifying the time of initial divergence. Here it is interesting to note that the differences between the two dimensional CJRM and the EGM3D are smaller and occur at later times than for the 2D and 3D pile temperature response analysis of Ref. 16. This is because we have used a more appropriate insulated surface boundary condition for our three dimensional analysis to reflect the position of most pile heat exchangers beneath a building. Whereas the resulting G-functions in Ref. 16 assume a constant surface temperature boundary more relevant for ground heat exchangers exposed to the ambient air temperature. The same constant temperature boundary condition is also used in other analytical models for piles e.g. Ref. 20.

In timescales longer than the three years considered in Fig. 8, semi-infinite GHE with an insulated upper boundary condition will eventually reach steady state at a time dependent on the pile AR, as shown in Ref. 19. However, as shall be seen in Section 3.2.2, a key factor for model errors in practice is the model differences at timescales corresponding to those when the thermal load changes. Hence, these very long timescale divergences are expected to be less important to practical model performance compared with daily and seasonal load fluctuations.

3.2.2. Variable thermal load

The temperature response of the two models under the conditions described in Fig. 3 are shown in Fig. 9 for both the rotary and CFA pile geometries. The specific cases are detailed in Table 1.

In all cases the absolute model differences in Fig. 9 are less than 1 °C, and for the majority of the year, less than 0.5 °C. For the rotary case (Fig. 9a to d) the maximum absolute difference between EGM3D and CJRM is 0.8 °C and occurs in cooling. For the CFA case (Fig. 9e to h) the corresponding maximum absolute difference is 0.7 °C, also in cooling. This is because the maximum cooling demand occurs at a higher peak power than the heating demand and temperature changes (and hence model differences) are proportional to applied heating power. For heating, the maximum absolute differences are 0.5 °C and for both rotary and CFA, reflecting lower peak heating power. In both these cases the same approximate magnitude of absolute difference is seen in the initial heating period and the final heating period. This is important as it shows no compounding of error with time over the year.

The maximum difference between the two models can also be considered in relative terms. Comparing the maximum absolute difference to the maximum absolute temperature changes in EGM3D gives 7 % to 16 % in the rotary case and 4 % to 8 % in the CFA case. In both cases the percentage errors start larger and reduce throughout the simulation. They are also proportional to the magnitude of the thermal demand, hence also being smaller in value for the majority of the year.

It is also worth noting that the patterns of temperature change predicted by CJRM and EGM3D are not the same for the CFA and the rotary cases due to the differing shapes of their respective G-functions. For the CFA case, the EGM3D, CJRM and difference curves all parallel each other (Fig. 9f, g, h). In heating the decrease in temperature is always under predicted by the CJRM compared with the EGM3D, while in cooling, the increase in temperature is also under predicted by CJRM.

For the rotary case, CJRM also initially under predicts the change in temperature due to imposition of each heating or cooling phase (Fig. 9b, c, & d). However, because the CJRM curve lags the EGM3D curve, this causes the curves to cross over. Hence as the heating or cooling demand reduces in each phase, so the CJRM comes to over predict the temperature reduction in heating and also over predict the temperature increase in cooling. This lag and crossing over is caused by the larger difference between the CJRM and EGM3D G-functions for the rotary case at around 1 to 2 h (Fig. 10), the timescale over which heating and cooling demand drops off rapidly (Fig. 3). In contrast, for the CFA case, the difference between the two G-functions is almost zero at this time, only increasing at larger time values.

3.3. Comparison of CJRM with real TRT data

A thermal response test in the London Clay for a $r_b = 300$ mm thermal pile has been reported in Ref. 19. The test lasted 353 h (14.7 days) and the pile was 31 m deep. Based on the temperature of the exchange fluid which was circulated prior to the test, the initial temperature in the pile and ground is estimated at 14.2 °C.

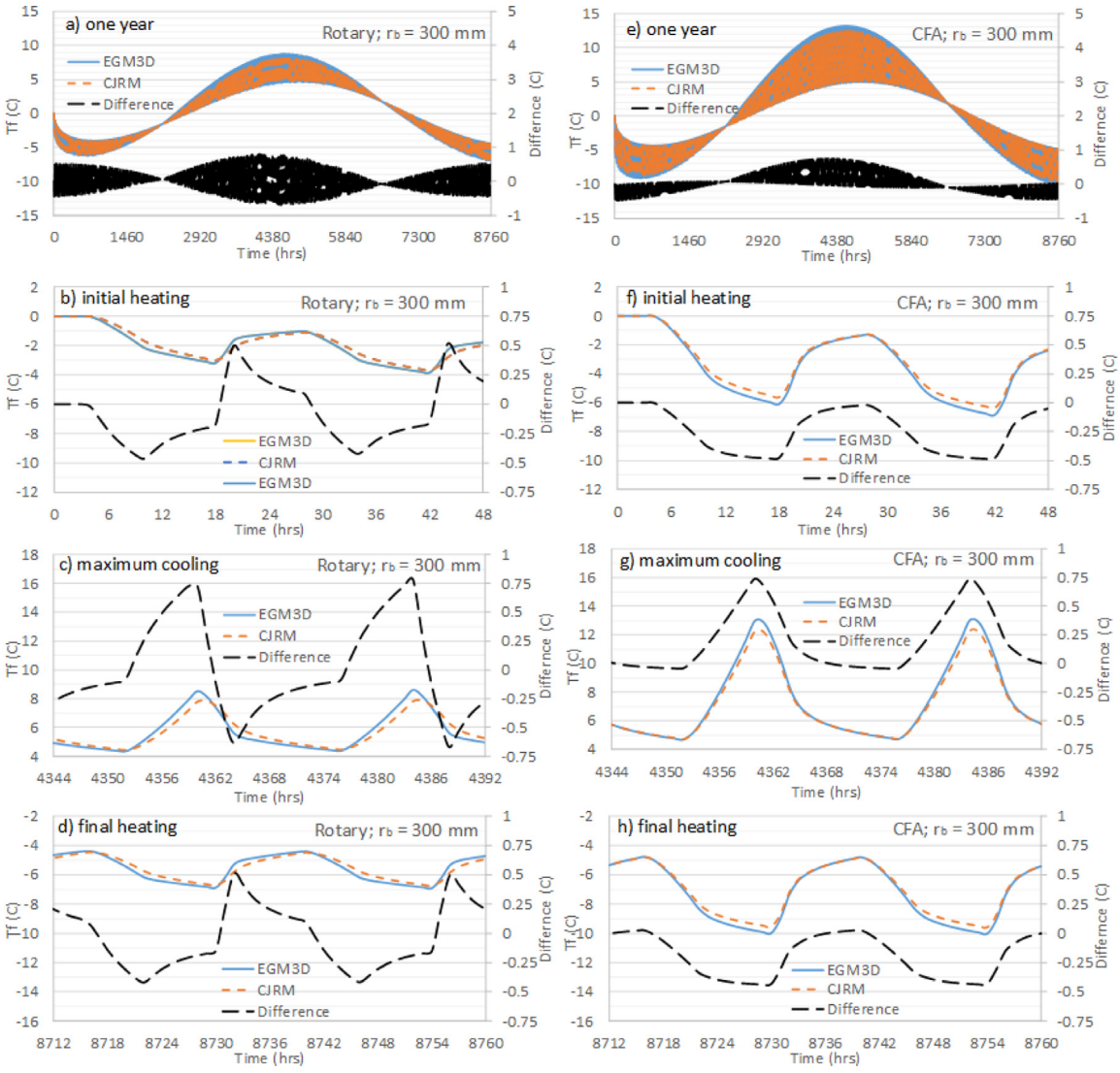

Fig. 9. Temperature change and model difference for a year long simulation of cyclic heating and cooling for Rotary (a, b, c, d) and CFA (e, d, g, h) piles with $r_b = 300$ mm, $N_p = 4$, $\lambda_c = 2$ W/mK, λ_g 1 W/mK. For the CJRM model, $\Delta t = 0.01$ hour. Temperature difference expressed as EGM3D-CJRM.

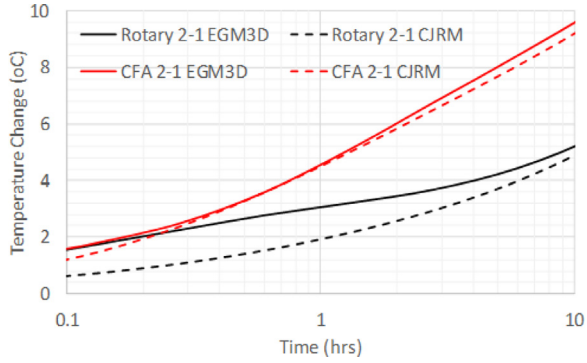

Fig. 10. Temperature response with time (G-function) for rotary and CFA piles with $r_b = 300$ mm, $N_p = 4$, $\lambda_c = 2$ W/mK, λ_g 1 W/mK, and $q_{inj} = 50$ W/m.

The pile has 4 pipes within it, separated by shank spacing of 42.5 cm. The applied thermal power was 1.69 kW. Full details of the test and material parameters are given in Table 2.

To fit these data only λ_c needs to be varied, since λ_g is uniquely defined by the late-time gradient of the TRT and has already been fitted by Ref. 19, who found a value of 1.48 W/mK using a 'resistive-capacitive' model. Rather than vary diffusivities directly, we fix the thermal capacities to match those estimated by Ref. 19 (i.e. $C_g = 2.4$ MK/Km^3 and $C_b = 2.2$ MK/Km^3).

By this approach, a good fit was achieved for the EGM3D for $\lambda_c = 0.88$ W/mK (with $r_{pe} = 0.138$ m and therefore $R_b = 0.14$ mk/W), with all the other parameters fixed (Fig. A.1). This compares to 0.94 W/mK estimated by Ref. 21. The shape of the thermal response curve also matches well with the experimental data.

Whilst correctly matching the asymptotes, the CJRM fit underestimates the field data for Fo <0.3 or t <10 h (Fig. 11). This mid time underestimate is consistent with the analysis shown in Fig. 6 and Fig. 7 for rotary piles. It would theoretically be possible to improve the fit by adjusting λ_c, whilst keeping constant the best-fit $R_b = 0.14$ mk/W. However, this route has not been pursued to maintain the physical basis of the approach, and avoid entrainment of errors related to the inherent uncertainties of real case data where the actual ground and concrete properties are not known with absolute precision.

Also shown on Fig. 11 are some traditional and pile ground heat exchanger models. The linear simplification and exponential integral form of the infinite line source model (ILS, Refs. 41, 43)

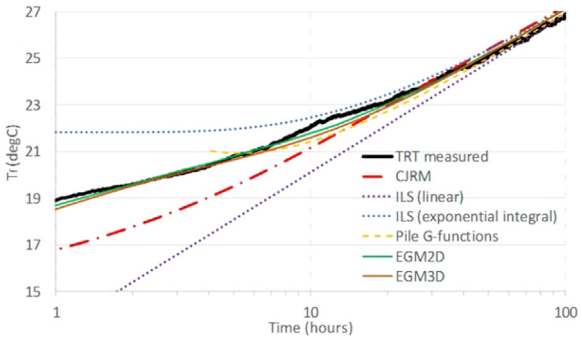

Fig. 11. Measured TRT data[19] compared to temperature response models using the parameters from Maragna & Loveridge 2019. CJRM is Claesson–Javed Radial model, ILS is Infinite Line Source, Pile G-Functions from Ref. 16, Explicit Geometry models in 2D and 3D are EGM2D, EGM3D.

plot beneath and above the early to mid-time data respectively. The pile G-functions[16] underestimate the temperature response for under 11 h, but overestimate the response at smaller times. The simulated temperature response curve is also markedly curved with an unrealistic upturn at the smallest time of its validity. This unrealistic shape has its origin in the semi-empirical relationship derived from curve fitting and perhaps suggests the need for adjustment to its validity times. The numerical models EGM2D and EGM3D are also shown in Fig. 11. The fit is good but includes discrepancies arising from the use of a constant power assumption in all the analysis, despite the fact that real power levels are subject to small fluctuations. These simulations also come with greater computational expense compared to the other models shown.

4. Discussion

This paper presents the application of a radially symmetric heat conduction model to energy piles with the aim of providing a fast run time, yet theoretically robust analytical approach for design of pile ground heat exchangers. The suitability of the model should be determined against a number of criteria: accuracy for different pile geometries in the short term, long term performance, and ease/speed of use.

Analysis of a wide range of geometries under constant thermal load suggests that the CJRM model will perform best for CFA piles. A good performance is also seen for rotary piles with four or more pipes installed, providing the pipe spacing is not too great. However, for small numbers of pipes, especially in larger piles, the equivalent radius approximation becomes less valid. For comparisons in two dimensions, for typical applied power values, a circumferential pipe spacing of less than 550 mm will keep the absolute error below 1 °C. This error may appear large, but it is reasonable when put in the context of expected ground loop temperature variations (±10 °C to 15 °C). Cases of larger diameter CFA piles, or rotary piles with many pipes will all have smaller associated errors, especially with favourable thermal conductivity values. All the greatest errors occurred where the pile concrete was less conductive that the ground. In the reverse scenario errors were often approximately half the magnitude.

The three dimensional comparison between models having a time-variable thermal load, at similar levels to those that may occur in practice, also showed reasonable agreement between CJRM and numerical simulations. Maximum difference between the two models were up to 0.8 °C and are associated with the times of peak power demand and also the greatest rate of change in power demand. Due to the computational demands of the EGM3D simulations, numerical errors mean that these differences may be underestimated slightly. Scaling the spatial discretisation errors described in Section 2.3.2 for the average thermal power applied in the heating and cooling phases of the analysis, suggests that CJRM errors could reach 0.9 °C in the worst case (rotary case with maximum power application). Nonetheless, for the majority of the year long simulation CJRM errors remained below 0.5 °C. Actual values in practice would depend on the pattern of applied thermal demand.

Errors appear largely consistent over a 1 year timescale under varying load conditions. While these short to medium term errors may be non-conservative, in the longer term any model differences will be conservative. At three years under constant thermal demand, only 5% model difference was observed, but with CJRM overestimating temperature changes compared with numerical simulation. In the longer term these two factors may cancel each other out. Additionally, these longer timescales do not correspond to critical changes in demand (hourly, daily, seasonal). Hence they may be less influential on overall model performance than smaller timescale model differences. The smaller impact of axial effects in the long term compared with previous studies also suggests that the assumption of an insulated surface boundary condition is a key difference between the operational conditions of energy piles and boreholes, making piles more suitable to two dimensional or quasi two-dimensional analysis than longer aspect ratio boreholes.

When compared with other energy pile design models the CJRM approach performs well. It gives a more appropriate temperature response than the line source equations. Due to its physical basis it also gives an improved temperature response curve compared with the empirical pile G-functions. While CJRM is more complicated to use than these latter simpler solutions, it can still be readily coded in Matlab or similar software (refer to Appendix for full equations for doing this), and also maintains fast run times. In this analysis, small time steps (0.01 h) were used for application of CJRM to avoid any temporal discretisation errors compared with the numerical simulations, but these may not be required in practice. By comparison with resistive capacitive models, CJRM is also a lot easier to use and based in a real physical geometry with no "black box" aspects.[44] By comparison with the fit of Ref. 19, the resistive capacitive model required 10 geometric based parameters, whereas the CJRM requires only determination of r_{pe} based on the pile resistance.

Finally, the use of CJRM may be compared with the application of numerical simulation which is increasingly available to even smaller companies. The process of validating CJRM in this study has again shown the computational challenge of running three dimensional numerical simulation with hourly varying loads over many years as would be required for design cases. Even with the use of high performance computing facilities, long term fully three dimensional analysis is challenging to complete and demonstrates the need for simple, robust and fast engineering solutions like CJRM.

5. Conclusions

The Claesson–Javed Radial Model (CJRM), originally developed for simulating borehole ground heat exchangers, has been tested for the case of energy piles, which have much larger diameters and thus smaller aspect ratios than typical boreholes. The step response of a thermal pile is dominated by the fluid thermal capacity at early time and by the ground resistance at late-time, transitioning between these, via a period dominated by ground heat exchanger resistance at mid-time. CJRM has been tested over all three of these time periods and the following conclusions are drawn:

- The CJRM can be matched asymptotically at early and late times. The deviation from simulations using an explicit geometry therefore occurs at 'mid-time'. The maximum deviation typically occurs between 1 h and 3 h and is less than 1 °C for typical applied power conditions, for CFA piles and for rotary piles with four or more pipes at circumferential spacing of less than 550 mm.
- For rotary piles the CJRM will always underestimate the temperature response function at mid time, while for CFA piles it may over estimate it.
- Errors of approximately 0.5 °C or less are obtained for larger diameter CFA piles, for rotary piles with many pipes and for cases of high concrete conductivity with respect to the ground conductance.
- The CJRM model requires very few fitting parameters, so is likely to be more robust than highly parameterised models requiring extensive inverse modelling.
- Fast run times can be achieved making the method suitable for use in practice.

Nomenclature

CJRM – Claesson–Javed Radial Model (analytical model); CS – circumferential separation of pipes; EGM – Equivalent Geometry Model; GHE – Ground Heat Exchanger; TRT – Thermal Response Test.

Greek Symbols

ρ Density (kg/m^3)
λ Thermal conductivity (W/mK)
Φ Dimensionless temperature ($=2\pi\,\Delta T_f/q$) (-)

Roman Symbols

A Cross-sectional area (m^2)
a Thermal diffusivity ($=\lambda/(\rho c)$) (m^2/s)
c Specific heat capacity (J/kgK)
C Thermal capacity per unit depth (J/mK)
d Thickness of pipe (m)
D_a Depth of aquifer (m)
D_b Depth of borehole/pile (m)
h Fluid convective heat transfer coefficient (W/m^{2}K)
Fo Fourier number (–)
N Number (w.r.t. pipes this means number of pipes counted over a horizontal cross-section) (–)
Q Power (W)
q Power per unit depth (W/m)
R Thermal Resistance (mK/W)
R_b Thermal Resistance of borehole (*i.e.* fluid to outer boundary of borehole) (mK/W)
R_c Thermal Resistance of GHE material (concrete or grout) (mK/W)
r Radial distance (m)
T Temperature (K)
t Time (s)
v Velocity (m/s)

Subscripts

0 Initial
c GHE filling material (typically concrete or grout for pile GHE)
f Heat-exchanger fluid
g Ground (soil)
i Inner
inj Injection
o Outer
p Pipe
pe Equivalent pipe (for the radial approximation)

CRediT authorship contribution statement

Fleur Loveridge: Conceptualization, Methodology, Resources, Data curation, Writing – original draft, Writing – review & editing, Visualization, Project administration, Funding acquisition. **Nicholas Woodman:** Methodology, Software, Validation, Formal analysis, Data curation, Writing – original draft, Writing – review & editing, Visualization. **Saqib Javed:** Methodology, Writing – review & editing. **Johan Claesson:** Methodology, Writing – review & editing.

Declaration of competing interest

The authors declare that they have no known competing financial interests or personal relationships that could have appeared to influence the work reported in this paper.

Acknowledgements

This work was supported under the EPSRC, UK grant EP/P001351/1, 'Non Steady Analytical Models for Energy Pile Testing and Design'. The authors acknowledge the use of the IRIDIS High Performance Computing Facility, and associated support services at the University of Southampton, in the completion of this work. In particular, we thank David Hempston for his indefatigable support.

All authors have read and agreed to the published version of the manuscript.

Data statement

The main G-functions presented in this paper and the Matlab code used to calculate temperature changes according to the CJRM analytical model are freely available from the University of Leeds research data repository at https://doi.org/10.5518/1167.

Appendix

The concept of the Claesson–Javed Radial Model is explained in Section 2.2, with full details and derivation given in Ref. 23. Fluid temperature is calculated with the following integral:

$$T_f(t) = \frac{2}{\pi}\cdot\int_0^\infty \frac{1-e^{-u^2\cdot\frac{t}{t_0}}}{u}\cdot L(u)\,du, \tag{A.1}$$

where,

$$L(u) = \mathrm{Im}\frac{-q_{inj}}{C_f\cdot\frac{-u^2}{t_0}+\frac{1}{R_p+\frac{1}{\overline{K}_{p(u)}+\frac{1}{\overline{R}_t(u)+\frac{1}{\overline{K}_c(u)+\overline{K}_g(u)}}}}}. \tag{A.2}$$

$L(u)$ is obtained from a sequence of composite of resistances in the thermal network displayed in Fig. A.1, where s is the Laplace variable and $t_0 s = -u^2$, for $0 < u < \infty$, and t_0 is an arbitrary time constant.[23] The conductances and corresponding resistances in the thermal network are given by the following expressions:

$$\overline{K}_g(u) = \frac{1}{\overline{R}_g(u)} = \frac{2\pi\lambda_g\cdot\tau_g u\cdot\left[J_1(\tau_g u)-i\cdot Y_1(\tau_g u)\right]}{J_0(\tau_g u)-i\cdot Y_0(\tau_g u)}, \tag{A.3}$$

$$\overline{K}_t(u) = \frac{1}{\overline{R}_t(u)} = \frac{4\lambda_c}{J_0(\tau_p u)\cdot Y_0(\tau_c u)-Y_0(\tau_p u)\cdot J_0(\tau_c u)}, \tag{A.4}$$

$$\overline{K}_p(u) = \frac{1}{\overline{R}_p(u)}$$

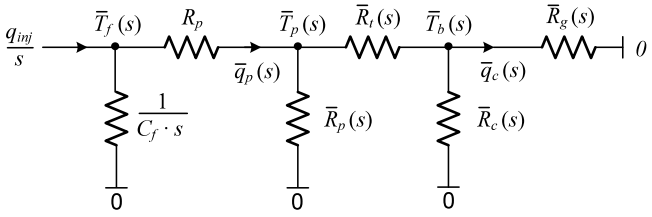

Fig. A.1. The thermal network relating the Laplace Transforms of the pipe, ground heat exchanger and ground, for solution of the CJRM equivalent ground heat exchanger, after[22]

$$= 4\lambda_c \cdot \frac{0.5 \cdot \pi \tau_p u \cdot \left[J_1\left(\tau_p u\right) Y_0\left(\tau_c u\right) - Y_1\left(\tau_p u\right) J_0\left(\tau_c u\right)\right] - 1}{J_0\left(\tau_p u\right) \cdot Y_0\left(\tau_c u\right) - Y_0\left(\tau_p u\right) \cdot J_0\left(\tau_c u\right)}, \tag{A.5}$$

$$\overline{K}_c(u) = \frac{1}{\overline{R}_c(u)}$$

$$= 4\lambda_c \cdot \frac{0.5 \cdot \pi \tau_c u \cdot \left[J_1\left(\tau_c u\right) Y_0\left(\tau_p u\right) - Y_1\left(\tau_c u\right) J_0\left(\tau_p u\right)\right] - 1}{J_0\left(\tau_p u\right) \cdot Y_0\left(\tau_c u\right) - Y_0\left(\tau_p u\right) \cdot J_0\left(\tau_c u\right)}, \tag{A.6}$$

$$\tau_p = r_p/\sqrt{a_c \cdot t_0},\ \tau_c = r_b/\sqrt{a_c \cdot t_0},\ \tau_g = r_b/\sqrt{a_g \cdot t_0}. \tag{A.7}$$

References

1. European Parliament. European parliament resolution of 14 2019 on climate change – A European strategic long-term vision for a prosperous, modern, competitive and climate neutral economy in accordance with the Paris agreement (2019/2582(RSP). 2019 Available at https://www.europarl.europa.eu/doceo/document/TA-8-2019-0217_EN.html. [Accessed 18 May 2020].
2. European Parliament. European parliament resolution of 15 2020 on the European green deal (2019/2956(RSP). 2020 Available at https://www.europarl.europa.eu/doceo/document/TA-9-2020-0005_EN.html. [Accessed 18 May 2020].
3. United Nations. Paris agreement. 2015 Available at https://unfccc.int/sites/default/files/english_paris_agreement.pdf. [Accessed 20 September 2019].
4. CCC. *Net Zero Technical Report*. Committee on Climate Change; 2019 2019, Available at https://www.theccc.org.uk/wp-content/uploads/2019/05/Net-Zero-Technical-report-CCC.pdf. [Accessed 20 September 2019].
5. CCC. Next steps for UK heat policy, committee on climate change. 2016 2016, Available at: https://www.theccc.org.uk/wp-content/uploads/2016/10/Next-steps-for-UK-heat-policy-Committee-on-Climate-Change-October-2016.pdf. [Accessed 3 June 2019].
6. CCC. Reducing UK emissions. Progress Report to Parliament; Committee of Climate Change; 2018 2018 Avaiable at https://www.theccc.org.uk/wp-content/uploads/2018/06/CCC-2018-Progress-Report-to-Parliament.pdf. [Accessed 20 September 2019].
7. Imperial College. Analysis of alternative UK heat decarbonisation pathways, for the committee on climate change. 2018 2018, Available at https://www.theccc.org.uk/wp-content/uploads/2018/06/Imperial-College-2018-Analysis-of-Alternative-UK-Heat-Decarbonisation-Pathways.pdf. [Accessed 18 May 2020].
8. IEA. Net zero by 2050, IEA, Paris. 2021 Available at: https://www.iea.org/reports/net-zero-by-2050. [Accessed 6 October 2021].
9. Lu Q, Narsilio GA. Cost effectiveness of energy piles in residential dwellings in Australia. *Curr Trends Civ Struct Eng*. 2019;3(3).
10. Loveridge F, Smith P, Powrie W. A review of design and construction aspects for bored thermal piles. *Ground Eng*. 2013;2013.
11. Zarrella A, De Carli M, Galgaro A. Thermal performance of two types of energy foundation pile: helical pipe and triple U-tube. *Appl Therm Eng*. 2013;61:301–310.
12. Wang D, Lu L, Zhang W, Cui P. Numerical and analytical analysis of groundwater influence on the pile geothermal heat exchanger with cast-in spiral coils. *Appl Energy*. 2015;160(705). 714.
13. CIBSE. Ground source heat pumps - CIBSE TM51. 2013 The Chartered Institution of Building Services Engineers, London, UK..
14. Laloui L, Sutman M. Energy geostructures: a new era for geotechnical engineering practice. In: *Proceedings of the XVII ECSMGE-2019 Geotechnical Engineering Foundation of the Future*. 2019 Available at https://www.ecsmge-2019.com/uploads/2/1/7/9/21790806/k5-1106-ecsmge-2019_lysse_keynote_paper.pdf. [Accessed 20 September 2019],
15. Bockelmann F, Fisch MN. It works—Long-term performance measurement and optimization of six ground source heat pump systems in Germany. *Energies*. 2019;12:4691.
16. Loveridge F, Powrie W. Temperature response functions (G-functions) for single pile heat exchangers. *Energy*. 2013;57:554–564.
17. Wood CJ, Liu H, Riffat SB. Comparison of a modelled and field tested piled ground heat exchanger system for a residential building and the simulated effect of assisted ground heat recharge. *Int J Low-Carbon Technol*. 2010;5(3):137–143.
18. Li M, Lai ACK. New temperature response functions (g-functions) for pile and borehole ground heat exchangers based on composite-medium-line-source theory. *Energy*. 2012;38:255–263.
19. Maragna C, Loveridge FA. A resistive-capacitive model of pile heat exchangers with an application to thermal response tests interpretation. *Renew Energy*. 2019;138:891–910. 2019.
20. Man Y, Yang H, Diao N. A new model and analytical solutions for borehole and pile ground heat exchangers. *Int J Heat Mass Transf*. 2010;53(13–14):253–2601.
21. Loveridge F, Powrie W. 2D thermal resistance of pile heat exchangers. *Geothermics*. 2014;50:122–135. 2014.
22. Javed S, Claesson J. New analytical and numerical solutions for the short-term analysis of thermal response tests used to measure ground thermal properties. *ASHRAE Trans*. 2011;117(1):13–21. 2011.
23. Claesson J. *Radial Heat Flow for a Pipe in a Borehole in Ground using Laplace Solutions*. Report on mathematical background; Goteborg, Sweden: Chalmers University of Technology, Report; 2011 2011:4, Available at, https://research.chalmers.se/en/publication/159856. [Accessed 6 August 2020],
24. Woodman N, et al. Evaluating the applicability of the radial approximation for pile heat exchangers. In: Ferrari EA, Laloui L, eds. *Energy Geotechnics: SEG 2018*. 2019:3–10. In: Springer Series in Geomechanics and Geoengineering..
25. Cullin JR, Spiter JD. A computationally efficient hybrid timestep methodology for simulation of ground heat exchangers. *Geothermics*. 2011;40:144–156.
26. Loveridge F, Cecinato F. Thermal performance of thermoactive continuous flight auger piles. *Environ Geotech*. 2016;3(4):265–279.
27. Eskilson P. *Thermal Analysis of Heat Extraction Boreholes* [Doctoral Thesis]. Sweden: Department of Mathematical Physics, University of Lund; 1987.
28. Zeng HY, Diao NR, Fang ZH. A finite line-source model for boreholes in geothermal heat exchangers. *Heat Transf Asian Res*. 2002;31(7):558. 567.
29. Rees S, Van Lysebetten G. A response factor approach to modelling long term thermal behaviour of energy piles. *Comput Geotech*. 2020;120:103424.
30. Thomas HR, Rees SW. Measured and simulated heat transfer to foundation soils. *Geotechnique*. 2009;59(4):365–375.
31. Mikhaylova O, Johnston IW, Narsilio GA. Ground thermal response to borehole ground heat exchangers. In: Wuttke F, Bauer S, Sanchez M, eds. *Energy Geotechnics: Proceedings of the 1st International Conference on Energy Geotechnics*. ICEGT 2016, Kiel, Germany, 2016:29–31. 2016.
32. Habert J, El'Mejahed M, Bernard J-B. Lessons learned from mechanical monitoring of a thermoactive pile. In: Wuttke F, Bauer S, Sanchez M, eds. *Energy Geotechnics: Proceedings of the 1st International Conference on Energy Geotechnics*. ICEGT 2016, Kiel, Germany, 2016:29–31. 2016.
33. BSI. Bs EN 1992-1-1:2004 - Design of concrete structures. 2004 General rules and rules for buildings.
34. Javed S, Spitler J. Accuracy of borehole thermal resistance calculation methods for grouted single U-tube ground heat exchangers. *Appl Energy*. 2017;187:790–806.
35. Loveridge F, McCartney JS, Narsilio GA, Sanchez M. Energy geostructures: A review of analysis approaches, in situ testing and model scale experiments. *Geomech Energy Environ*. 2020;22:100173, 2020.
36. Cecinato F, Loveridge FA. Influences on the thermal efficiency of energy piles. *Energy*. 2015;82:1021–1033. 2015.
37. SIA. *Utilisation de la Chaleur Du Sol Par Des Ouvrages de Fondation Et de Soutenement En Beton, Guide Pour la Conception, la Realisation Et la Maintenance*. Swiss Society of Engineers and Architects; 2005 Documentation D 0190.
38. Bennet J, Claesson J, Hellstrom G. *Multipole Method to Compute the Conductive Heat Flow to and Between Pipes in a Composite Cylinder*. Report; Lund, Sweden: University of Lund, Department of Building and Mathematical Physics.; 1987.
39. Claesson J, Javed S. Explicit multipole formulas and thermal network models for calculating thermal resistances of double U-pipe borehole heat exchangers. *Sci Technol Built Environ*. 2019;25(8):980–992.
40. Claesson J, Javed S. Explicit multipole formula for the local thermal resistance in an energy pile - the line-source approximation. *Energies*. 2020;13(5445).

41. Carslaw HS, Jaeger JC. *Conduction of Heat in Solids*. second ed. Oxford University Press.; 1959.
42. Loveridge F, Powrie W. Pile heat exchangers: thermal behaviour and interactions. *Proc Inst Civ Eng Geotech Eng*. 2013;166(2):178–196.
43. Beier RA, Smith MD. Borehole thermal resistance from line-source model of in-situ tests. *ASHRAE Trans*. 2002;108:212–219. 2002.
44. Maragna C, Loveridge F. A new approach for characterizing pile heat exchangers using thermal response tests. *Energies*. 2021;14(12):3375. http://dx.doi.org/10.3390/en14123375, 2021.